Investigation into the role of macrophages heterogeneity on solid tumour aggregations

Eftimie, Raluca

Published in:
Mathematical Biosciences

DOI:
10.1016/j.mbs.2020.108325

Publication date:
2020

Noname manuscript No.
(will be inserted by the editor)

Investigation into the role of macrophages heterogeneity on solid tumour aggregations

R. Eftimie

Received: date / Accepted: date

Abstract Macrophages are one of the most important immune cell populations that can be found inside solid tumours. For a long time, it was thought that these cells have an anti-tumour role, but relatively recent research has shown that they can have both anti-tumour and pro-tumour roles as determined by their phenotypes. Due to the heterogeneity and plasticity of macrophage population, with cells changing their phenotypes in response to the tumour microenvironment, it is difficult to fully understand their role inside the solid tumours. Here we consider a mathematical modelling and computational approach to investigate the change in macrophages phenotypes (either determined by the tumour itself, or by external interventions) on overall tumour growth/control/decay. To this end we consider two simple models: one focusing on two extreme phenotypes (the M1 anti-tumour cells, and the M2 pro-tumour cells), and one considering a macrophage population structured by a continuous phenotype variable. We investigate their asymptotic dynamics (through steady-state analysis), as well as their transient behaviours (through numerical simulations). We show that while a re-polarisation of the phenotype of macrophages, as considered by many recent experimental studies, can lead to tumour control, for tumour elimination it is required that macrophages are fully functional (i.e., the rate at which they kill tumour cells is high). We also show that a mixed macrophage's phenotype can keep the tumour under control in a state of dormancy. Moreover, an increase in this mixed phenotype can cause a delay in tumour reduction (accompanied by a larger tumour reduction), as well as a delay in tumour relapse.

Keywords M1 and M2 macrophages · Structured population model · Tumour-immune interactions

R. Eftimie
Mathematics, University of Dundee, Dundee, DD1 4HN
Tel.: +44(0)1382 384488
E-mail: r.a.eftimie@dundee.ac.uk

1 Introduction

More and more experimental studies emphasise the importance of tumour-macrophage interactions on the progression of malignant tumours [2,11,46,47, 49,70]. One reason is that macrophages can represent between 5-40% of solid tumour mass [64,66]. For years it was thought that macrophages, as immune cells, have an anti-tumour role [19,20]. However, experimental studies over the last 20-30 years have shown that macrophages are a very heterogeneous and plastic cell population, which can eliminate tumours as well as help them grow larger. The heterogeneity of macrophages, with phenotypes varying from the anti-tumour classically-activated M1 cells to the pro-tumour alternatively-activated M2 cells (see also Fig.1), makes it difficult to understand and control their roles in tumour progression, especially when macrophages express markers characteristic to both activation states (i.e., M1 and M2) [47,49].

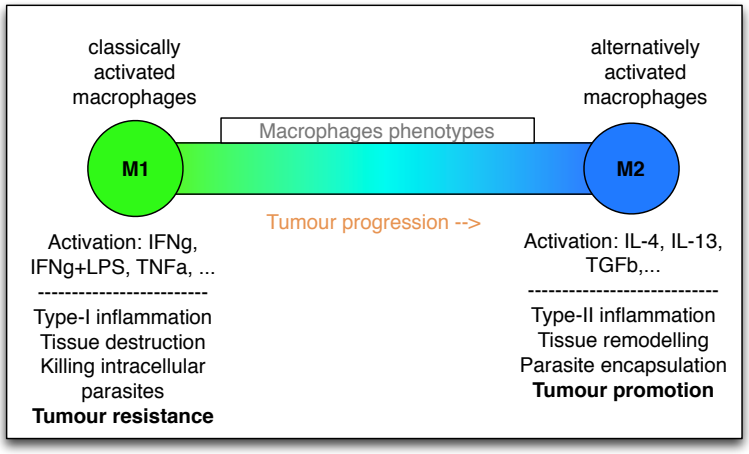

Fig. 1 The two extreme macrophage phenotypes are represented by the M1 and M2 cells. However, between them there is a continuous range of phenotypes. As tumour progresses, it induces macrophages re-polarisation from mainly a M1 phenotype towards a M2 phenotype.

In this study we focus on breast cancer (i.e., the 4T1 murine breast cancer cell line), which is associated with very large numbers of macrophage infiltrates that can form up to 40% of tumour mass [14,45,66]. Many experimental studies on breast cancers have shown a M1→M2 polarisation of macrophages co-cultured with 4T1 cells [41,46,64,71]. The M2 cells were also associated with a fast tumour proliferation [64]. The poor prognosis of tumours with large macrophages infiltrates, combined with the plasticity of macrophages (i.e., these cells can change their phenotype in response to the environment they are in) lead researchers to suggest a M2→M1 macrophage re-polarisation as a way of treating cancers [24,32,49]. In fact, recent experimental studies have shown that the re-polarisation of M2 macrophages towards an M1-like

phenotype (e.g., by antibody targeting as in [25]) can inhibit breast cancer progression. Moreover, there are studies suggesting that the 4T1 breast cancer cells, which secrete extracellular vesicles up-taken by macrophages, can in fact prime the tumour-associated macrophages towards an M1-like phenotype [43]. This result could probably be explained by the mixed M1/M2 phenotypes of macrophages infiltrates in some solid tumours [45]. In fact, these mixed M1/M2 phenotypes are quite common in various cancers: from breast cancers [45], to prostate cancers [60], ovarian cancers [59], pancreatic cancers [35], lung cancers [63], skin cancers [3]. The differentiation of these macrophages with mixed phenotypes, which express markers corresponding to the M1 phenotype (e.g., HLA-DR^{hi}, CD11, CD80) as well as markers corresponding to the M2 phenotype (e.g., HLA-DR^{lo}, CD206, CD163), is the result of various tumour-derived factors [35], and allows the macrophages to adjust to their environment. However, despite the phenotypic characterisation of macrophage populations infiltrating various tumours (sometimes using markers that might not always be perfect indicators of the extent of cell polarisation [59]), the role of these mixed-phenotype macrophages on tumour progression is still not fully understood.

Here, we consider a mathematical approach to investigate the effect of injecting a number of cancer cells into a mouse (as done in various experimental setups [28]; see also Fig. 2), which leads to the accumulation of macrophages with different phenotypes inside the tumour microenvironment. The mathematical studies published in the literature focus mainly on the effect of the two extreme types of macrophages, M1 and M2 cells, on tumour evolution; see [4, 15,16,39,40,44,52,57]. However, as mentioned above, the tumour-associated macrophages have a continuous range of phenotypes, with many cells expressing markers characteristics of both M1 and M2 phenotypes [2,45]. This aspect, which is missing from the mathematical literature, will be addressed in this study. In particular, we will use the mathematical models derived in this study to better understand the impact that the number of immune cells with mixed phenotypes vs. immune cells with single phenotypes could have on the growth/control/elimination of tumour cells. We will also investigate the impact of changes in macrophages polarisation/re-polarisation rates, either induced by normal tumour progression or by external treatment [32,49], as well as changes in the rates at which M1-like macrophages eliminate tumours [34], on the overall growth/control/elimination of these tumour cells. In particular, we will show that tumour control (dormancy) can occur in the presence of macrophages with mixed phenotypes that have medium anti-tumour activities.

We acknowledge that the tumour microenvironment contains multiple types of immune cells (e.g., CD8$^+$ and CD4$^+$ T cells, B cells, granulocytes [14]) that interact directly or indirectly with the macrophages, and thus can influence their dynamics. However, to keep the mathematical model as simple as possible, and to identify the main mechanisms behind tumour growth/control/decay, here we focus only on the macrophage population.

We start in Section 2 with the description of two mathematical models for tumour-macrophages interactions: a model that focuses on the two dis-

crete extreme macrophage phenotypes (M1 and M2), and a model that considers the phenotype as a continuum variable which induces a structure in the macrophage population. In Section 3 we investigate the transient and asymptotic dynamics of these two models by focusing on both numerical simulations and stability analysis of steady states. We summarise and further discuss the results in Section 4.

2 Model description

To develop the mathematical model for tumour-macrophage interactions, we use a step-by-step approach. In subsection 2.1 we focus on a simple model for the dynamics of the two extreme types of macrophages, M1 and M2 cells, and their interactions with the tumour cells inside the tumour micro-environment. Then, in subsection 2.2 we combine the two equations for the M1 and M2 populations into one equation for the macrophages structured by the phenotype variable $m \in [0, L_m]$ (with $m = 0$ describing the pure M1 cells, and $m = L_m$ describing the pure M2 cells). Both mathematical models describe a hypothetical experimental protocol summarised in Fig. 2 (which follows the steps of many experimental protocols [5]), where a certain number of tumour cells are injected into a mice and a few days later we start to investigate the tumour-immune dynamics. It should be mentioned that the subcutaneous injection of cancer cells into the mice (see classical experimental murine protocols [28, 53]) leads to an inflammatory microenvironment which attracts (within 48 hours [8]) the M1 macrophages. Thus, for both models below, we assume that at the initial time there is a tumour population and a M1-like macrophage population.

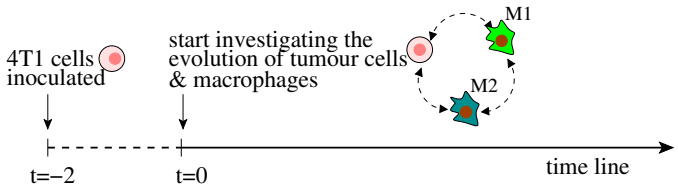

Fig. 2 A hypothetical experiment investigated in this study. We assume that a number of breast tumour cells have been inoculated into the system, and 2 days later (when the tumour has started growing and has attracted the M1 pro-inflammatory macrophages) we start investigating the dynamics of tumour-immune interactions.

2.1 Discrete phenotype macrophage populations

For simplicity, we start by assuming that the macrophage population is represented by the 2 extreme phenotype cells: the anti-tumour M1 cells and the

pro-tumour M2 cells. The dynamics of the tumour-immune interactions is described by the following equations:

$$\frac{du_T}{dt} = p_t u_T\Big(1 - \frac{u_T}{K_T}\Big)\big(1 + r_m u_{M2}\big) - d_t u_T u_{M1}, \tag{1a}$$

$$\frac{du_{M1}}{dt} = p_{m1} u_{M1}\Big(1 - \frac{u_{M1} + u_{M2}}{K_M}\Big) - d_m u_{M1} - \alpha_{m1} u_{M1}\frac{u_T}{u_T + K_T^*} + \alpha_{m2} u_{M2}, \tag{1b}$$

$$\frac{du_{M2}}{dt} = p_{m2} u_{M2}\Big(1 - \frac{u_{M1} + u_{M2}}{K_M}\Big) - d_m u_{M2} + \alpha_{m1} u_{M1}\frac{u_T}{u_T + K_T^*} - \alpha_{m2} u_{M2}. \tag{1c}$$

This model incorporates the following assumptions:

- In equation (1a) we assume that the tumour cells proliferate at a baseline rate p_t, following a logistic growth law with carrying capacity K_T, to account for a slow-down in growth at larger sizes due to a lack of nutrients [37]. Tumour proliferation rate is increased (at a rate r_m) by the presence of M2-like macrophages, which were shown in [69] to contribute to the growth of breast cancer cells following their co-culture. Finally, the tumour cells can be eliminated at a rate d_t by the anti-tumour M1-like macrophages (via antibody-dependent cell phagocytosis [29]). Since tumour cells are usually long-lived (with limitless replicative potential and evasion of programmed cell death being two of the hallmarks of cancers [30]), in this study we decided to ignore the death rate of cancer cells. This makes sense in the context of 4T1 cells that can spontaneously metastasise [58], despite the fact that in general tumour cell survival is a rate-limiting step in cancer metastasis [68].
- The M1 macrophages in equation (1b) are recruited and proliferate at a rate p_{m1}, up to a carrying capacity K_M. This assumption of logistic growth is made to describe the typical experimental growth curves of macrophages, which show an exponential phase followed by a stationary phase; see [10]. In addition, the assumption that the logistic term describes both recruitment and proliferation is made since it is currently not clear if all tumour-associated macrophages are derived from blood monocytes recruited to the tissue, or derived from embryonic macrophages that locally proliferate in the tissue, or both [70]. Also, having only one term that describes both recruitment and proliferation allows us to avoid introducing another parameter into the model.
  Returning to the description of terms in equation (1b), we assume that the M1 macrophages can die at a rate d_m. They can re-polarise at a rate α_{m1} into M2 cells in response to signalling molecules, such as IL10, TGF-β, that are secreted by the tumour cells [62]. To avoid an unrealistically large M1→M2 re-polarisation in the presence of large tumours, we used a saturated term with K_T^* a constant for the level of tumour cells (or cytokines/chemokines produced by these cells) that trigger this

re-polarisation. We also assume that the M2 cells can re-polarise into M1 cells at a smaller rate α_{m2} in the presence of molecules such as IFN-γ secreted by other anti-tumour cells in the environment, e.g., NK cells, $CD8^+$ T cells [23]. This M2→M1 re-polarisation could also be induced externally with the aim of reducing tumour progression [25].
– The M2 macrophages can proliferate in a logistic manner at a rate p_{m2}. For simplicity, throughout this study we assume that $p_{m1} = p_{m2} =: p_m$. Again, for simplicity (and because we do not have any data to support other assumptions), we assume that the M2 cells have a similar half-life as the M1 cells (and therefore they die at a rate d_m). The re-polarisation rates have been discussed above.

2.2 Continuous phenotype macrophage population

Consider now the following coupled ODE-PDE model for the dynamics of tumour cells, $u_T(t)$, and a phenotype-structured macrophage population $u_M(m,t)$, $m \in [0, L_m]$ (with u_M being the sum of the previous M1 and M2 cell populations):

$$\frac{du_T(t)}{dt} = p_t u_T(t)\Big(1 - \frac{u_T(t)}{K_T}\Big)\Big(1 + r_m \int_0^{L_m} H_2(m) u_M(m,t) dm\Big) - d_t u_T(t) \int_0^{L_m} H_1(m) u_M(m,t) dm, \tag{2a}$$

$$\frac{\partial u_M}{\partial t} + \frac{\partial\big(\gamma(t) u_M F(u_T, u_M)\big)}{\partial m} = p_m u_M(m,t)\Big(1 - \frac{u_M(m,t)}{K_M}\Big) - d_m u_M(m,t), \tag{2b}$$

with the re-polarisation function $F(u_T, u_M)$ defined as

$$F(u_T, u_M) = \alpha_{m1} \frac{u_T(t)}{u_T(t) + K_T^*} - \alpha_{m2} \int_0^{L_m} H_2(m) u_M(m,t) dm, \tag{3}$$

where the first term models the re-polarisation (at rate α_{m1}) of u_M cells towards a M2-like phenotype in the presence of u_T cells, while the second term models the re-polarisation (at rate α_{m2}) of u_M cells towards a M1-like phenotype. The re-polarisation speed $\gamma(t)$ is defined as a decreasing function of the M2-like macrophages, to model the situation where once the macrophages acquired the M2 phenotype (i.e., $\int_0^{L_m} H_2(m) u_M(m,t) dm$ is large), the movement through the phenotype space slows down very fast:

$$\gamma(t) = e^{-g_0 \int_0^{L_m} H_2(m) u_M(m,t) dm}. \tag{4}$$

Here, g_0 is a slow-down index for macrophages' progression through the phenotype space. This slow-down index models the assumption that while initially

macrophages re-polarise quickly away from the $m = 0$ phenotype (under the influence of tumour cells), this re-polarisation slows down after the cells acquire a mixed phenotype. This assumption is supported by experimental studies that emphasise the fast acquisition of mixed phenotypes by many tumour-associated macrophages; for example, in [35] the authors have seen that after 72hr of differentiation, more than 90% of macrophages had a mixed phenotype polarisation. Of course, if the immune cells have mostly a M1-like phenotype, then $\gamma(t) \approx 1$ and the speed of M1→M2 re-polarisation will be determined by α_{m1}.

The right-hand-side of equation (2b) for macrophages was obtained by adding the two ODEs (1b) and (1c) for the extreme M1 and M2 phenotypes (and therefore it incorporates similar assumptions as for model (1)). Note that the logistic growth is assumed to depend only on the macrophage population with the same phenotype m. This is because the M1-like cells lead to the production of type-1 cytokines (e.g., IFN-γ secreted by Th1 $CD4^+$ T cells [55]) that can trigger the further differentiation and growth of M1-like cell population [1,6], while the M2-like cells lead to the production of type-2 cytokines (e.g., IL-4 secreted by Th2 $CD4^+$ T cells [55]) that can trigger the further differentiation and growth of M2-like cell population [1]. The two kernels $H_1(m)$ and $H_2(m)$ that appear on the right-hand-side of equation (2a) describe the phenotype ranges that characterise the M1 and M2 cells. Throughout this study we will consider two cases (although we discuss the impact of different types of kernels in Appendix D):

– There is a distinct separation between the phenotypes of cells considered to be M1 or M2, which can be described by step-wise kernels (see also Fig.3(a)):

$$H_1(m) = \begin{cases} \frac{2}{L_m}, & \text{for } 0 \le m \le \frac{L_m}{2} \\ 0, & \text{for } m > \frac{L_m}{2} \end{cases} \quad \text{and} \quad H_2(m) = \begin{cases} 0, & \text{for } 0 \le m \le \frac{L_m}{2} \\ \frac{2}{L_m}, & \text{for } m > \frac{L_m}{2} \end{cases} \tag{5}$$

– There is an overlap between the phenotypes of cells considered to be M1 or M2, which can be described by the following kernels (see also Fig. 3(b)):

$$H_1(m) = \begin{cases} \frac{2}{L_m+2\epsilon}, & \text{for } 0 \le m \le \frac{L_m}{2} + \epsilon \\ 0, & \text{for } m > \frac{L_m}{2} + \epsilon \end{cases}$$
$$\text{and} \quad H_2(m) = \begin{cases} 0, & \text{for } 0 \le m \le \frac{L_m}{2} - \epsilon \\ \frac{2}{L_m+2\epsilon}, & \text{for } m > \frac{L_m}{2} - \epsilon \end{cases} \tag{6}$$

Here, ϵ gives the degree of overlap between the phenotype kernels H_1 and H_2: for $\epsilon = 0$, equations (6) reduce to (5).

In the following we investigate the behaviour of models (1) and (2), by starting in Section 3.1 with the asymptotic dynamics described by the steady states, under the assumption that the system approaches a "quasi-equilibria", where the tumour and macrophage populations don't vary much. Then, we continue in Section 3.2 with the investigation of the transient dynamics of the

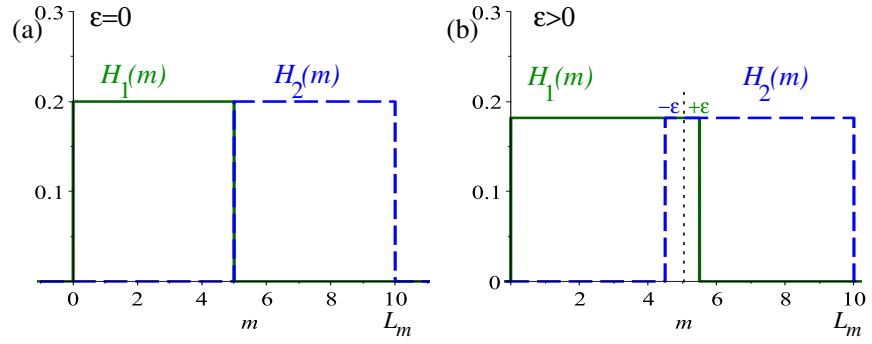

Fig. 3 (a) Distinct step-wise kernels (5) defined on two distinct intervals over the phenotype domain: $[0, L_m/2]$ and $[L_m/2, L_m]$, where we consider an arbitrary phenotype domain length $L_m = 10$. (b) Overlapping step-wise kernels (6), which have similar values in the middle of the phenotype domain over the range of $[L_m/2 - \epsilon, L_m/2 + \epsilon]$.

systems, as given by the numerical simulations. The parameter values used for these results are summarised in Table 1 in Appendix A.

3 Results

3.1 Steady states and their linear stability

To investigate the long-term dynamics of models (1) and (2), we focus on the steady states (given by $\frac{du_T}{dt} = \frac{du_{M1}}{dt} = \frac{du_{M2}}{dt} = 0$, and $\frac{du_T}{dt} = \frac{du_M}{dt} = \frac{du_M}{dm} = 0$) and their local stability.

We need to emphasise that in the context of cancer-immune interactions, when we refer to these steady states we actually mean "quasi-steady states". When the tumour is present, a quasi-equilibrium means that the tumours doesn't change significantly its size at least for some time after it consumes the available nutrients [36,37] (and thus it undergoes an angiogenic dormancy [17]), or when it is controlled by the immune cells during the process of immune-mediated dormancy [17,67]. In the absence of tumours, the quasi-equilibrium is characterised by macrophages that perform surveillance tasks [50].

3.1.1 Extreme-phenotype case: model (1)

Model (1) can exhibit the following 5 types of steady states (whose stability is discussed in more detail in Appendix B):

1. $(u_T^*, u_{M1}^*, u_{M2}^*) = (0, 0, 0)$, which is always unstable (see Appendix B);
2. $(u_T^*, u_{M1}^*, u_{M2}^*) = (0, K_M \frac{p_m - d_m}{p_m}, 0)$, with $p_m > d_m$. This state is unstable if $p_t p_m > d_t K_M (p_m - d_m)$ (see Appendix B);
3. $(u_T^*, u_{M1}^*, u_{M2}^*) = (0, u_{M1}^* > 0, u_{M2}^* > 0)$ which exists only when $p_{m1} \neq p_{m2}$ (see Appendix B). This case is not considered in this study, where we assume (for simplicity) that $p_{m1} = p_{m2} = p_m$.

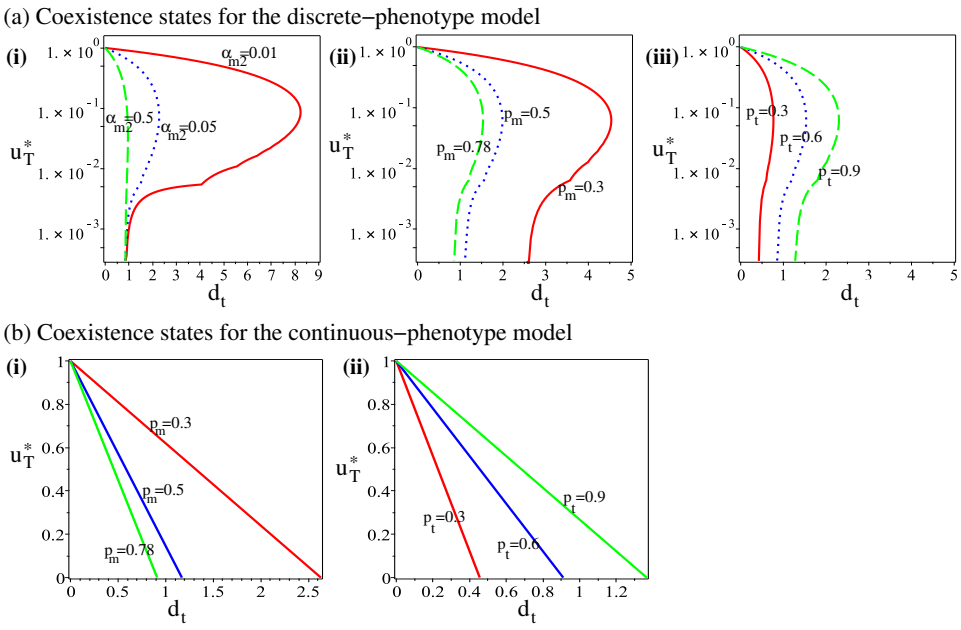

Fig. 4 (a) Coexistence steady state ($u_T^* > 0, u_{M1}^* > 0, u_{M2}^* > 0$) for the discrete phenotype model (1). We show the tumour state u_T^* as a function of d_t as we vary (i) α_{m2}; (ii) p_m; (iii) p_t. (b) Coexistence steady state ($u_T^* > 0, u_M^* > 0$) for the continuous phenotype model (2). We show the tumour state u_T^* as a function of d_t, while we vary (i) p_m; (ii) p_t. All other parameters are fixed at their baseline values in Table 1.

4. $(u_T^*, u_{M1}^*, u_{M2}^*) = (K_T, 0, 0)$, which is unstable if $p_m > d_m$ (see Appendix B);
5. $(u_T^* > 0, u_{M1}^* > 0, u_{M2}^* > 0)$ given by $u_{M1}^* = K_M(p_m - d_m)/p_m - u_{M2}^*$, and u_{M2}^* and u_T^* satisfying the following two coupled equations:

$$u_{M2}^* = \frac{\left(\frac{\alpha_{m1}(p_m - d_m)K_M}{pm}\frac{u_T^*}{K_T^* + u_T^*}\right)}{\left(\alpha_{m2} + \alpha_{m1}\frac{u_T^*}{K_T^* + u_T^*}\right)}, \tag{7a}$$

$$0 = p_t\left(1 - \frac{u_T^*}{K_T}\right)(1 + r_m u_{M2}^*) - d_t\left(\frac{(p_m - d_m)K_M}{p_m} - u_{M2}^*\right). \tag{7b}$$

In regard to the parameter regions where this coexistence steady state exists, in Fig. 4(a) we graph u_T^* as a function of various parameters. When d_t is small, there is always one steady state with large u_T^*, irrespective of the values of α_{m2}, p_t or p_m (or any other model parameters). For intermediate d_t, there could be two co-existence steady states: one with a high tumour population and one with a relatively low tumour population, which can be considered as a dormant tumour state (being kept under control by the M1 cells). For large d_t there is no co-existence state, as the tumour will always be eliminated.

We will return to this discussion at the end of Section 3.2.1, in the context of numerical simulations. Moreover, for the stability of this coexistence state, see Fig. 9 in Appendix B.

It is not possible to have a steady state formed of tumour cells and only one macrophage phenotype (i.e., $u^*_{M2} > 0$ & $u^*_{M1} = 0$; or $u^*_{M2} = 0$ & $u^*_{M1} > 0$). In the presence of the tumour, there must always be some level of M1 and M2 cells in the system. This result is consistent with the experimental observation that solid tumours contain macrophages with mixed M1/M2 phenotypes [45]. A less realistic steady state is the tumour-only state. To ensure that this state is never reached, in this study we focus only on those p_m and d_m values such that $p_m > d_m$.

3.1.2 Continuous phenotype case: model (2)

In regard to the phenotypic-homogeneous steady states $u_T(t) = u^*_T$, $u_M(m,t) = u^*_M = const.$, it can be easily shown that model (2) exhibits the same steady states as model (1) after we add the M1 and M2 populations:

1. $(u^*_T, u^*_M) = (0,0)$, which is always unstable (see Appendix C);
2. $(u^*_T, u^*_M) = (0, K_M \frac{p_m - d_m}{p_m})$, which is asymptotically stable provided that $p_m p_t < d_t K_M(p_m - d_m) - p_t r_m K_M(p_m - d_m)$ (see Appendix C);
3. $(u^*_T, u^*_M) = (K_T, 0)$, which is asymptotically unstable when $p_m > dm$ (for all phenotypic wavenumbers; see Appendix C);
4. (u^*_T, u^*_M) given explicitly by

$$u^*_M = K_M(p_m - d_m)/p_m, \quad \text{and} \tag{8a}$$

$$u^*_T = (K_T/p_t)\big(p_t(1 + r_m u^*_M) - d_t u^*_M\big)/(1 + r_m u^*_M). \tag{8b}$$

This state, which exists for $p_m > d_m$ and $p_t p_m + K_M(p_t r_m - d_t)(p_m - d_m) > 0$, is always asymptotically stable (for all phenotypic wavenumbers; see Appendix C). Note that the condition for the existence of this state is the same as the instability condition for the state $(0, u^*_M > 0)$. In Fig. 4(b) we graph u^*_T as a function of d_t for different values of p_t and p_m (which influence the existence of this state).

Remark 1 *To describe the asymptotic dynamics of model (2), one needs to calculate the phenotypically-heterogeneous steady states $(u^*_T, u^*_M(m))$, which are given by equations*

$$u^*_T = \frac{K_T}{p_t}\Big[\frac{p_t\big(1 + r_m \int_0^{L_m} H_2(m) u^*_M(m) dm\big) - d_t \int_0^{L_m} H_1(m) u^*_M(m) dm}{1 + r_m \int_0^{L_m} H_2(m) u^*_M(m) dm}\Big],$$

$$\frac{du^*_M(m)}{dm} = \frac{u^*_M(m)}{\gamma^* F(u^*_T, u^*_M)}\Big[(p_m - d_m) - \frac{p_m}{K_M} u^*_M(m)\Big],$$

where

$$\gamma^* = e^{-g_0 \int_0^{L_m} H_2(m) u^*_M(m) dm},$$

and

$$F(u_T^*, u_M^*) = \alpha_{m1} \frac{u_T^*}{u_T^* + K_T^*} - \alpha_{m2} \int_0^{L_m} H_2(m) u_M^*(m) dm.$$

These states could be further simplified if we assume that there is no tumour (i.e., $u_T^* = 0$; see also the simulations in Section 3.2.2). However, a closed-form phenotypically-heterogeneous solution is difficult to obtain even in this case due to the integral terms in $F(0, u_M^*)$, and thus a numerical approach has to be considered when calculating these states. Fig. 5 shows an example of a phenotypically-heterogeneous state, which corresponds to the asymptotic dynamics of the numerical simulations in Fig. 7(c').

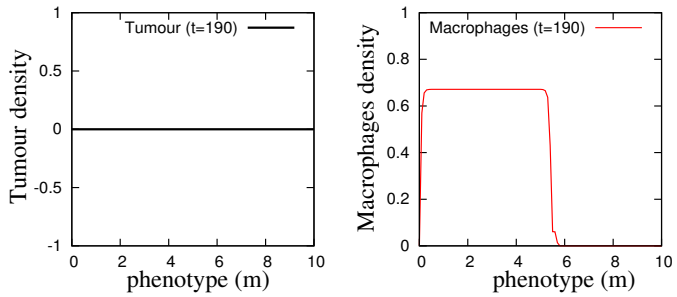

Fig. 5 Time snapshot of a state with no tumour (u_T^*) and a phenotypically-heterogeneous macrophage population ($u_M^*(m)$). The simulations were obtained with model (2), for the parameter values listed in the caption of Fig. 7(c').

3.2 Numerical results

In the following, we focus on the transient behaviour of models (1) and (2), and investigate the effect of various parameters on tumour growth/decay. As initial conditions for the ODE model (1) we choose $u_T(0) = 0.05$, $u_{M1}(0) = 0.001$, $u_{M2}(0) = 0.00037$. To propagate the solution at the next time step, we use a classical Runge-Kutta finite difference discretisation method.

Regarding the structured-population model (2), we assume that a small number of cells are introduced into the environment at $t = 0$, $u_T(0) = 0.05$ (same as for the discrete-phenotype case), which leads to the activation and recruitment of macrophages with a dominant M1 phenotype (i.e., the peak of the $u_M(m)$ distribution is closer to $m = 0$ than to $m = L_m$):

$$u_M(m, 0) = 0.03 e^{-15(m - L_m/10)^2}, \text{ with } L_m = 10. \tag{9}$$

We chose the initial conditions for the structured macrophage population such that $\frac{1}{L_m} \int_0^{L_m} u_M(m, 0) dm = u_{M1}(0) + u_{M2}(0)$. To simulate numerically the solution of (2), we first discretise the integrals using Simpson's method. Then

we use an operator-splitting approach to deal with the advection term describing the transport through the phenotype m-space (which is discretised using a second-order MacCormack finite difference scheme), and with the reaction term describing cells proliferation/death (which is discretised using again a 4th order Runge-Kutta scheme). Finally, since we work on a bounded phenotype domain, we use no-flux boundary conditions.

In the following two subsections we investigate numerically the effects of two model parameters that are usually varied through immunotherapies, but are still not fully understood:

- The tumour-killing rate d_t, which might vary since it depends, for example, on the amount of membrane M-CSF present on the target tumour cells [33], or the PD-1 expression of tumour-associated macrophages which inhibits phagocytosis [27]. However, as emphasised in [48], the detailed mechanisms of tumour cell phagocytosis are not completely understood at this moment.
- The M2→M1 re-polarisation rate α_{m2}, which has been investigated experimentally and clinically over the past few years, with numerous macrophage re-polarising molecules being identified [12]. However, many of these re-polarising molecules are not able to generate durable tumouricidal effects [12]. Examples of molecules that have been show to lead to anti-tumour activities are microRNA-155 [7], acidic polysaccharides [38], or GM-CSF [18].

3.2.1 Numerical simulation of the discrete-phenotype model

Given that many experimental studies focus on methods to re-program tumour-associated macrophages towards an anti-tumour phenotype [12,21,24], in Fig. 6 we investigate the interplay between α_{m2} (the M2→M1 re-polarisation rate) and d_t (the killing rate of tumour cells by M1-like macrophages). Since various experimental studies discuss tumour progression in terms of the ratio of M1/M2 cells infiltrating solid tumours as well as the total numbers of infiltrating macrophages [9,31,42,56], in sub-panels (ii) we graph the percentage of M1 and M2 cells in the tumour environment (on the left vertical axis), and their total numbers/densities (on the right vertical axis). We emphasise that tumour growth can occur in the presence of a large number of M2 cells (Fig. 6(a)(i)), or large numbers of M1 cells (Fig. 6(b)(i)). Increasing the re-polarisation rate α_{m2} (Figs. 6(b)(i) and (d)(i)), to simulate the effect of tumour-associated macrophages' re-polarisation towards M1-like cells, does not automatically lead to tumour elimination if the macrophages had deficient phagocytosis described by low d_t. Increasing the rate d_t leads to tumour control (even when $u_{M2} > u_{M1}$; panel (c)), or even tumour elimination (when $u_{M1} > u_{M2}$ and $d_t > 1$). Note that tumour elimination occurs when the system approaches the steady state $(0, u^*_{M1}, 0)$, as the tumour-present state ceases to exist (see Fig. 4(a)), thus pushing the system towards the stable tumour-free state.

In the following we investigate numerically the case of a continuous phenotype space, where we can understand better the anti-tumour/pro-tumour effects of macrophages with mixed phenotypes, as described by model (2)+(5)+(6).

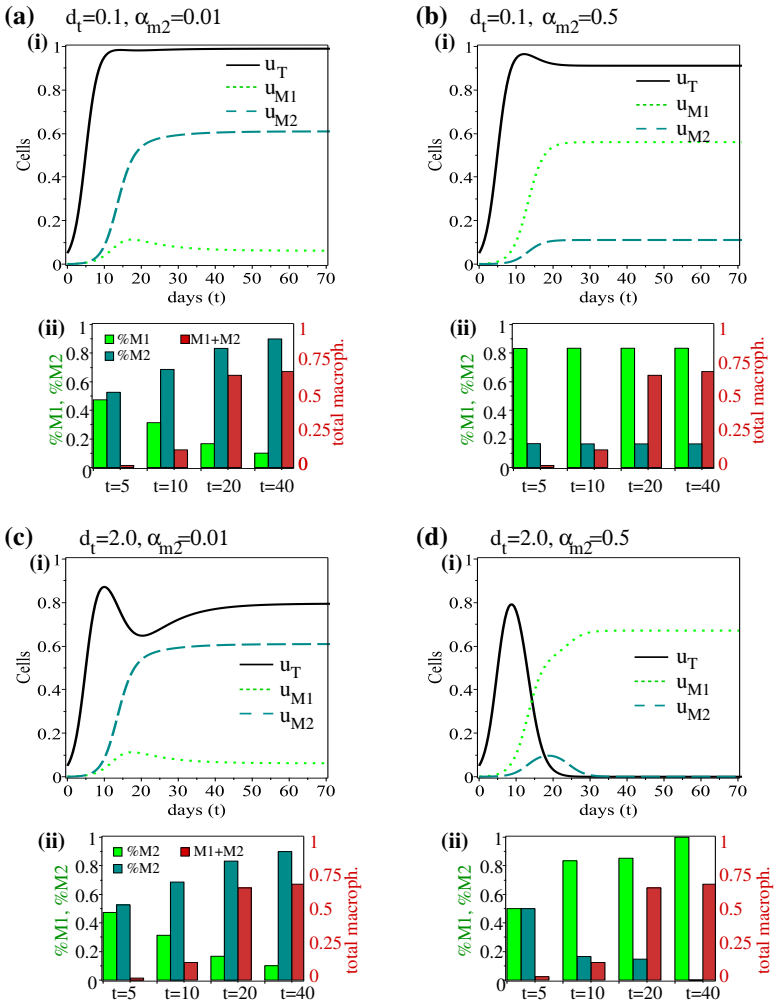

Fig. 6 Short-term dynamics of model (1), as we vary α_{m2} and d_t. Sub-panels (i) show the time-evolution of u_T, u_{M1} and u_{M2}, while sub-panels (ii) show the percentages of M1 and M2 cells on the primary (left) vertical axis, and the total number of macrophages on the secondary (right) vertical axis.

3.2.2 Numerical simulations of the continuous-phenotype model

To investigate the pro-tumour/anti-tumour effects of macrophages with distinct or mixed phenotypes, we focus on the two types of phenotype kernels described in Fig. 3, as we vary d_t and α_{m2}.

– *Step-wise kernels (5) for distinct M1-M2 phenotype separation.* In Fig. 7(a)-(c) we show the dynamics of model (2) as we assume that $\alpha_{m1} \gg \alpha_{m2}$ and vary the rate d_t. For a small d_t (see Fig. 7(a)) tumour grows towards its

carrying capacity, being helped by the macrophages which evolve towards an M2-like phenotype (i.e., $m > L_m/2 = 5$). As we increase d_t we see first a temporary reduction in tumour size (Fig. 7(b)), and eventually a complete tumour elimination (Fig. 7(c)) characterised by M1-like macrophages in the tumour microenvironment. Note that this M1-like phenotype is induced by the shrinking tumour (as $\alpha_{m1} \gg \alpha_{m2}$).
In Fig. 7(a')-(c') we increase the re-polarisation rate α_{m2} such that $\alpha_{m2} \gg \alpha_{m1}$, and we observe that a high α_{m2} combined with a low d_t slows down the M1→M2 re-polarisation, but it cannot control tumour growth (sub-panels (a')). Combining a large α_{m2} with a large d_t (sub-panels (b'),(c')) induces a shift in the macrophage phenotype, which leads to tumour elimination. This also leads to an accumulation of macrophages at the left boundary (due to the no-flux boundary conditions), and thus the system approaches a tumour-free heterogeneous-phenotype macrophage state, as in Fig. 5. Tumour elimination is associated with the disappearance of the tumour-present/macrophage-present state (8) caused by large d_t (which also induces a change in the stability of this coexistence state; see Appendix C). The very high levels of d_t required to control/eliminate the tumour (compared to the discrete-phenotype case) are the results of low total macrophage density (i.e., $u_M^* \approx 20\% u_T^*$).

– *Step-wise kernels (6) with phenotype overlap.* We assume that there is no perfect delimitation between the M1 and M2 cells (or actually, their anti-tumour/pro-tumour effects, in the sense that even the M1-like cells could carry some M2 markers). In Fig. 8 we graph the dynamics of model (2) under the assumption that $\alpha_{m1} \gg \alpha_{m2}$, and $d_t = 2$. It is clear that increasing the phenotype overlap leads to a delay in tumour reduction (but a greater reduction), as well as a delay in tumour relapse.

4 Summary and Discussion

While there are many mathematical studies in the literature that focus on the two extreme macrophage phenotypes, M1 and M2, our study is one of the very few that focus on both discrete and continuous phenotypes. Here, we introduced two simple models for tumour-macrophage interactions, where we considered: (i) a macrophage population with two extreme phenotypes (M1 and M2) which could re-polarise in response to tumour-secreted cytokines or growth factors, or in response to external actions, and (ii) a phenotype-structured macrophage population. We used these models to investigate the mechanisms involved in tumour growth/control/elimination, as well as the importance of considering discrete vs. continuous macrophages phenotypes in tumour progression.

We first compared the models in terms of the steady states they exhibit, and showed that while the re-polarisation rates α_1 and α_2 impact the type and stability of the steady states for the model with discrete phenotypes, they do not have any significant effect on the states exhibited by the model

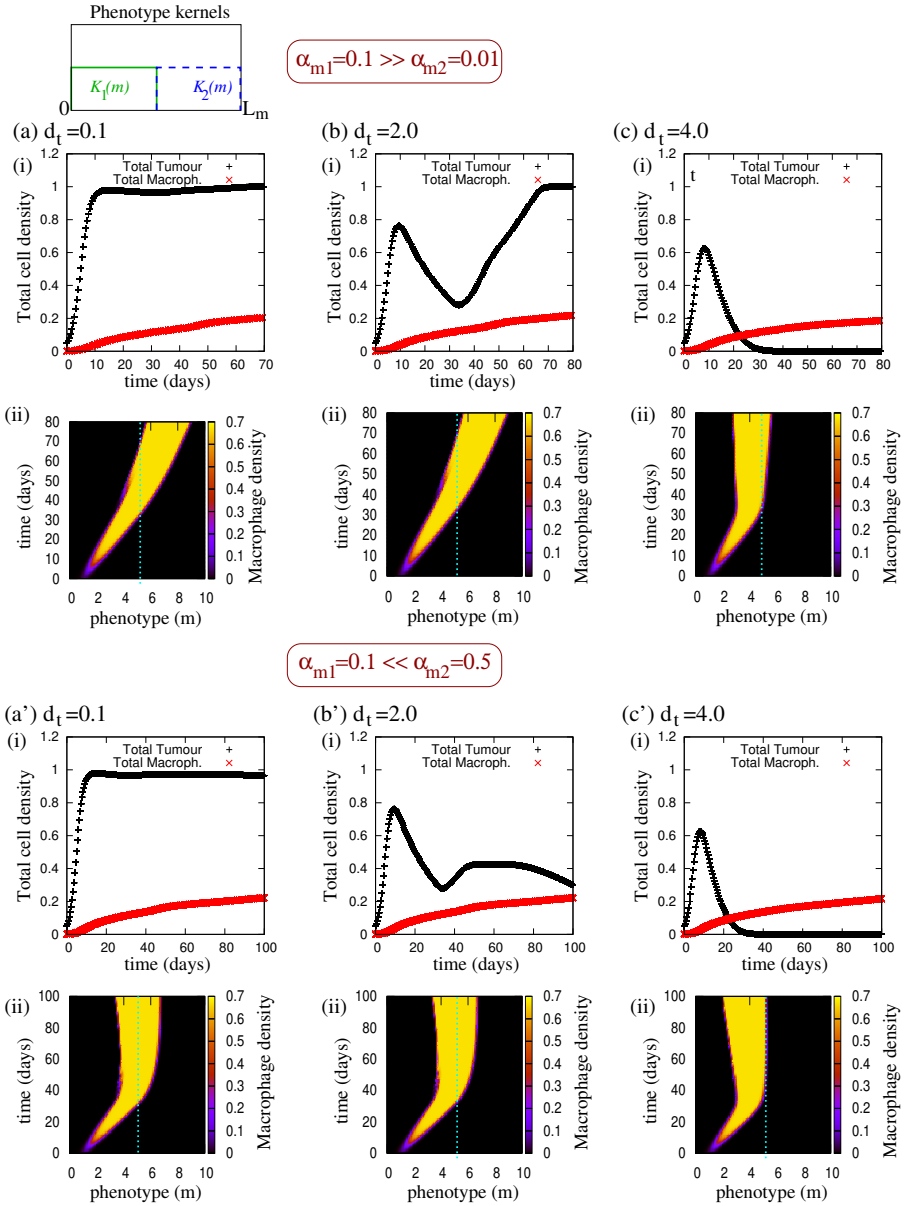

Fig. 7 Dynamics of system (2) with phenotype kernels (5) when: (a)-(c) we fix $\alpha_{m1} = 0.1 \gg \alpha_{m2} = 0.01$ and vary d_t, and (a')-(c') we fix $\alpha_{m1} = 0.1 \ll \alpha_{m2} = 0.5$ and vary d_t: (a),(a') $d_t = 0.1$, (b),(b') $d_t = 2.0$, (c),(c') $d_t = 4.0$. Sub-panels (i) show the total tumour density $u_T(t)$ and total macrophages density: $u_M(t) = \int_0^{Lm} u_M(m,t)dm$; sub-panels (iii) show the evolution of macrophages density in the (m,t) space. Dotted vertical line in sub-panels (iii) show the threshold phenotype $m = \frac{L_m}{2} = 5$, which separates the anti-tumour (M1) macrophages from the pro-tumour (M2) macrophages. Parameter values are: $p_t = 0.6$, $p_m = 0.7$, $d_m = 0.23$, $K_M = K_T = 1.0$, $K_T^* = 0.01$, $r_m = 0.1$, $g_0 = 1.5$.

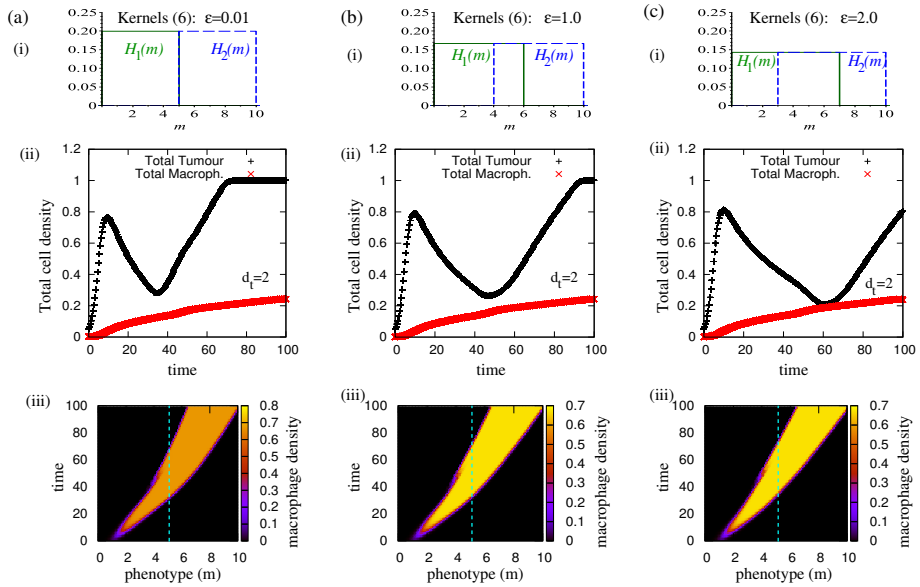

Fig. 8 Dynamics of system (2) with phenotype kernels (6), as we vary the overlap between M1 and M2 phenotypes of macrophages: from (a) $\epsilon = 0.01$, to (b) $\epsilon = 1.0$ and (c) $\epsilon = 2.0$. Sub-panels (i) show the kernels $H_{1,2}(m)$ for different ϵ; sub-panels (ii) show the total tumour and macrophages density; sub-panels (iii) show the phenotype distribution of macrophages during the evolution of tumour cells.

with continuous phenotype (because in this case, the re-polarisation rates were assumed to impact the movement through the phenotype space, and therefore they appeared only in the heterogeneous-phenotype steady states). Moreover, for the discrete-phenotype case we also showed that it was possible to have multiple tumour-macrophages coexistence states: with high tumour densities and low tumour densities; see Fig. 4(a). The low tumour branches correspond to the case of immune-mediated tumour dormancy, as the M1 cells controlled the growth of the tumour. The existence of these multiple co-existent states for the discrete-phenotype case was in contrast with the continuous-phenotype case where there was only one tumour-macrophage co-existence steady state; see Fig. 4(b). It should be emphasised here that the shape of the phenotype kernel did not have any impact on the type or stability of the phenotype-homogeneous steady states displayed by model (2); see also the discussion in Appendix C.

The numerical simulations for the discrete phenotype and continuous phenotype (with distinct kernels) showed relatively similar dynamics: tumour growth towards maximum size, temporary tumour control, or tumour elimination. Tumour elimination was the result of the disappearance of the coexistence state, which for the continuous phenotype model coincided also with the loss of stability of this state. (For the coexistence steady states with discrete phenotypes it was difficult to obtain an analytical condition for the loss of their

stability, to connect it with the analytical condition for the existence of these states.) For the models introduced in this study, a M2→M1 re-polarisation – which is one of the methods currently used in experiments to promote tumour regression [12,24] – could not lead to tumour elimination unless it was accompanied by an increase in the phagocytosis rate of tumour cells by macrophages (i.e., an increase in d_t, which can be obtained experimentally, for example, via monoclonal antibodies [29] or via an inhibition of PD-1 expression by tumour-associated macrophages [27]). This suggests that a combined therapeutic approach involving both a M2→M1 re-polarisation as well as an increase in phagocytosis might improve the current therapeutic outcomes.

The continuous phenotype model also showed tumour dormant behaviours, which occurred for large macrophage phagocytosis rates (d_t) in the context of mixed macrophages phenotypes; see Fig. 7(b'). In this case, for the parameter values considered in this study (see Table 1) the tumour was always eliminated as the M1-like phenotype won over the M2-like phenotype. Our theoretical study hypothesises that this immune-mediated dormancy is associated with the evolution of macrophage phenotype from an initial M1-like phenotype to a mixed M1/M2 phenotype. This aspect will have to be investigated experimentally since at this moment there are very few studies in the literature that focus on the phenotype of TAMs during tumour dormancy. Among these few experimental studies we mention [69], which suggests that the M1 macrophages may contribute to dormancy behaviours in metastatic breast cancer cells. However, in [69] it is not investigated whether those M1 macrophages could have also mixed phenotypes.

By focusing our attention on the amount of overlap between M1 and M2 markers, described in the model by the overlap between the kernels $H_1(m)$ and $H_2(m)$, we showed that a larger markers' overlap can lead to a delay in the reduction of tumours, as well as a delay in tumour relapse; see Fig. 8. Unfortunately, few experimental studies quantify the number/percentage of tumour-associated macrophages with mixed phenotypes; see [3,60]. If such experimental studies will be performed more often in the future, they could be used to inform the choice of phenotype kernels. This is particularly important since the simulations in Figs. 7-8 and Fig. 11 in Appendix D showed that the type of phenotype kernel can influence the rate at which the tumour is eliminated or grows back.

We need to emphasise that the models introduced in this study are very simple. For example, we assumed that the M1 and M2 proliferation rates could be described by an average value p_m, and their death rates could be described by an average value d_m. (This assumption allowed us to go from model (1) to model (2).) In the absence of any data to suggest otherwise, this was an acceptable assumption. However, given the different phenotypes and functions of the tumour-associated macrophages, it also raises the question of whether the proliferation/death rates could depend on the phenotype. More experiments need to be performed on macrophages turnover, before we clarify this aspect.

More complex tumour-macrophage interactions, and interactions between macrophages and other immune cells in the tumour microenvironment, e.g., $CD4^+$ or $CD8^+$ T cells, will be considered in future studies. Also, multiscale approaches will be developed to connect this cell-scale model with molecular dynamics that will help us understand better the functionality of M1 macrophages.

Acknowledgements R.E. acknowledges useful comments made by the reviewers, who helped improve this manuscript.

A Parameter values

Table 1 summarises the values of the parameters used throughout this study to simulate the dynamics of model (1). For simplicity, we have re-scaled the cell populations by their carrying capacities. This leads also to a re-scaling of the following parameters: $\tilde{r}_m = r_m K_M$, $\tilde{d}_t = d_t K_M$, $\tilde{K}_M = 1$, $\tilde{K}_T = 1$ and $\tilde{K}_T^* = \frac{K_T^*}{K_T}$. Now $\tilde{K}_T^*$, $\tilde{K_T}$, $\tilde{K}_M$, and r_m are dimensionless, while $\tilde{d}_t$ has units of $1/time$. All other parameters kept their original units. For simplicity, in Table 1 we ignore the tilde symbol ˜ for the rescaled parameters, but specify in the third column the units for these parameters (as well as the units for the unscaled parameters).

Regarding the parameters that kept their units, we made the following assumptions:

- We focus on breast cancer, and use the information from [28,53,72] to approximate p_t. Note that in [53], five different breast cancer cell lines were derived from one cancer patient (with stage I invasive ductal carcinoma), and then injected into BALB/c mice. The doubling times for all these clones were between $24 - 36$ hours [53], which implies a proliferation rate of $p_t \in \big(\frac{ln(2.0)}{36} \times 24, \frac{ln(2.0)}{24} \times 24\big)$/day=(0.46/day,0.69/day). Other breast cancer cell lines (also injected in BALB/c mice) have different doubling times, which can vary greatly between experiments. For example, the doubling time of 4T1 breast cancer cells (usually used to study stage IV human breast cancer) was shown to vary from $14.7 - 15$ hours (i.e., $p_t \approx 1.1$/day) in [72] to more than 4.3 days (i.e., $p_t \approx 0.16$) in [28]. Therefore, in this study we consider an average tumour proliferation rate $p_t = 0.6$/day.
- Unlike the tissue-resident macrophages that can persist for weeks and even months [26, 61], the tumour-associated macrophages have a very rapid turnover of less than 5 days [54,65]. In this study, we consider a TAM half-life of 3 days, corresponding to a death rate $d_{m1} = d_{m2} = d_m \approx 0.23$/day.
- Regarding macrophage proliferation, in [10] the authors observed that primary bone marrow derived macrophages have a doubling time of 20 hrs, while the splenocyte derived macrophages have a doubling time of 30 hrs. This translates into a proliferation rate $p_m \in (\ln(2.0)/30\text{hr}, \ln(2.0)/20\text{hr}) \approx (0.55, 0.83)$/day. For the numerical simulations we consider an averaged rate $p_m = 0.7$/day.

In regard to the dimensional (and non-dimensional) values value of K_T and K_T^*, note that in [22] the authors suggested that the tumour diagnostic level is between $10^7 - 10^9$ cells. In mice, tumours are considered lethal if they are larger than 1cm^3, which corresponds to a maximum of $\approx 10^9$ cells [13,51]. Thus, we can assume that the dimensional carrying capacity for a murine tumour is $K_T = 10^9$. Since at diagnostic (i.e. $\approx 10^7$ cells) the tumours are already infiltrated with macrophages, we assume that the maximum tumour level that triggers a M1→M1 polarisation is $K_T^* = 10^7 = 1\% K_T$. Following the re-scaling of cell populations by their carrying capacities, we obtained the non-dimensional values K_T and K_T^* shown in Table 1 (see also the discussion about the re-scaled cell populations, at the beginning of this Appendix A).

Table 1 Summary of parameters used for model (1). Since many parameters were varied over some ranges, in parentheses we show the baseline values used throughout this study. We chose these baseline values to describe tumour growth towards carrying capacity, so that we can investigate mechanisms that lead to tumour control/elimination.

Param.	Values; for rescaled model	Units (rescaled model)	Description & reference
p_t	0.16-1.0 (0.6)	$\frac{1}{time}$	Proliferation rate of tumour cells [53,72,28]
K_T	1	-	Carrying capacity of tumour cells
K_T^*	0.01	-	Tumour level that triggers a M1→M2 macrophages re-polarisation
r_m	0.1	-	Contribution of M2 macrophages to the proliferation of tumour cells
d_t	0.1-3.0 (0.1)	$\frac{1}{time}$	Elimination rate of tumour cells by M1 macrophages
p_{m1}=p_{m2}=p_m	0.5-0.9 (0.7)	$\frac{1}{time}$	Proliferation rate of M1 and M2 macrophages [10]
K_M	1	-	Carrying capacity of macrophages
d_{m1}=d_{m2}=d_m	0.13-0.69 (0.23)	$\frac{1}{time}$	Half life of M1 and M2 macrophages [54,65]
α_{m2}	0.01-0.5 (0.01)	$\frac{1}{time}$	Re-polarisation rate of M2 macrophages towards the M1-phenotype
α_{m1}	0.1-0.5 (0.1)	$\frac{1}{time}$	Re-polarisation rate of M1 macrophages towards the M2-phenotype
L_m	10	space	Length of the phenotype domain
g_0	1.5	-	Slow-down index for movement though the phenotype space

B Stability of steady states for model (1)

The Jacobian matrix associated with the ODE system (1) (at a generic steady state $(u_T^*, u_{M1}^*, u_{M2}^*)$) is

$$J = \begin{pmatrix} p_t\left(1-\frac{u_T^*}{K_T}\right)(r_m u_{M2}^*+1) - \frac{p_t u_T^*(r_m u_{M2}^*+1)}{K_T} - d_t u_{M1}^* & -d_t u_T^* & p_t r_m u_T^*\left(1-\frac{u_T^*}{K_T}\right) \\ -\frac{\alpha_{m1}u_{M1}^*}{K_T^*+u_T^*} + \frac{\alpha_{m1}u_{M1}^* u_T^*}{(K_T^*+u_T^*)^2} & p_m\left(1-\frac{u_{M1}^*+u_{M2}^*}{K_M}\right) - \frac{p_m u_{M1}^*}{K_M} - d_m - \frac{\alpha_{m1}u_T^*}{K_T^*+u_T^*} & -\frac{p_m u_{M1}^*}{K_M} + \alpha_{m2} \\ \frac{\alpha_{m1}u_{M1}^*}{K_T^*+u_T^*} - \frac{\alpha_{m1}u_{M1}^* u_T^*}{(K_T^*+u_T^*)^2} & -\frac{p_m u_{M2}^*}{K_M} + \frac{\alpha_{m1}u_T^*}{K_T^*+u_T^*} & p_m\left(1-\frac{u_{M1}^*+u_{M2}^*}{K_M}\right) - \frac{p_m u_{M2}^*}{K_M} - d_m - \alpha_{m2} \end{pmatrix}$$

Proposition 1 *Consider model (1) with the two extreme macrophage phenotypes, which can exhibit three steady states with neither macrophages nor tumour cells, or with only macrophages, or with only tumour cells.*

1. *The tumour-free macrophages-free steady state* $(0,0,0)$ *is always unstable.*
2. *The tumour-free M2-present steady state* $(0, \frac{(p_m-d_m)K_M}{p_m}, 0)$*, which exists only for* $p_m > d_m$*, is asymptotically stable if and only if* $p_m p_t < d_t K_M(p_m - d_m)$*.*

3. *The tumour-present macrophages-free steady state* $(K_T, 0, 0)$ *is asymptotically stable if and only if* $p_m < d_m$.

Proof:

1. The eigenvalues of the Jacobian matrix at the steady state $(0,0,0)$ are $\lambda_1 = p_t > 0$, $\lambda_2 = p_m - d_m$, and $\lambda_3 = p_m - d_m - \alpha_{m2}$. Since $\lambda_1 > 0$, this steady state is always unstable.
2. The eigenvalues of the Jacobian matrix at the steady state $(0, \frac{(p_m - d_m)K_M}{p_m}, 0)$ are $\lambda_1 = -(p_m - d_m) < 0$, $\lambda_2 = -\alpha_{m2} < 0$ and
$$\lambda_3 = \frac{-d_t K_M (p_m - d_m) + p_t p_m}{p_m}.$$
Therefore, the steady state $(0, \frac{(p_m - d_m)K_M}{p_m}, 0)$ is asymptotically stable if $\lambda_3 < 0$ and unstable if $\lambda_3 > 0$.
3. The eigenvalues of the Jacobian matrix at the steady state $(K_T, 0, 0)$ are $\lambda_1 = -p_t < 0$, $\lambda_2 = -(d_m - p_m)$, and
$$\lambda_3 = -\frac{K_T(\alpha_{m1} + \alpha_{m2}) + (K_T + K_T^*)(d_m - p_m) + \alpha_{m2} K_T^*}{K_T^* + K_T}.$$
Since for $d_m > p_m$ all eigenvalues are negative, the steady state $(K_T, 0, 0)$ is asymptotically stable. The state is unstable when $p_m > d_m$.

Remark 2 *The stability of the tumour-present and macrophages-present state* $(u_T^*, u_{M1}^*, u_{M2}^*)$ *is more difficult to be studied analytically in terms of all model parameters. Of course, we could simplify a bit the determinant* $|J - \lambda \mathbb{I}| = 0$ *(e.g., by adding 3rd row to the 2nd row, and the subtracting 2nd column from the 3rd column):*

$$\begin{aligned} &|J(u_T^*, u_{M1}^*, u_{M2}^*) - \lambda \mathbb{I}| = \\ &= -[(p_m - d_m) + \lambda] \begin{vmatrix} -\frac{p_T u_T^*(1 + r_m u_{M2}^*)}{K_T} - \lambda & p_t r_m u_T^* \left(1 - \frac{u_T^*}{K_T}\right) + d_t u_T^*, \\ \frac{\alpha_{m1} u_{M1}^*}{K_T^* + u_T^*} - \frac{\alpha_{m1} u_{M1}^* u_T^*}{(K_T^* + u_T^*)^2} & -\alpha_{m2} - \frac{\alpha_{m1} u_T^*}{K_T^* + u_T^*} - \lambda \end{vmatrix} \end{aligned} \tag{10}$$

which leads to one obvious eigenvalue $\lambda_1 = -(p_m - d_m)$. *However, the other two eigenvalues are the roots of the quadratic equation:*

$$\lambda^2 + \lambda C_1 + C_2 = 0, \quad \textit{with}$$

$$C_1 = \frac{p_t u_T^*(r_m u_{M2}^* + 1)}{K_T} + \alpha_{m2} + \frac{\alpha_{m1} u_T^*}{K_T^* + u_T^*} > 0$$

$$C_2 = \frac{p_t u_T^*(r_m u_{M2}^* + 1)}{K_T} \left(\alpha_{m2} + \frac{\alpha_{m1} u_T^*}{K_T^* + u_T^*}\right) - \frac{\alpha_{m1} u_{M1}^* u_T^* K_T^*}{(K_T^* + u_T^*)^2} \left[p_t r_m \left(1 - \frac{u_T^*}{K_T}\right) + d_t\right]$$

To have at least one of these eigenvalues positive, we require $C_2 < 0$, *or equivalently*

$$\frac{d_t}{K_T - u_T^*} \left(\alpha_{m2} + \frac{\alpha_{m1} u_T^*}{K_T^* + u_T^*}\right) < \frac{\alpha_{m1} K_T^*}{(K_T^* + u_T^*)} \left(p_t r_m u_T^* (1 - \frac{u_T^*}{K_T}) + d_t u_{M1}^*\right)$$

By looking at the above inequality, one could say that this inequality cannot hold for α_{m2} *large. However, given that* u_T^* *depends on model parameters and implicitly on* α_{m2} *(through equations (7)), it is difficult to obtain a clear understanding of the stability of this coexistence state in terms of various model parameters (and whether stability correlates with the existence of this state – as we will see in Appendix C for model (2)). However, we can fix model parameters (e.g., to the values in Table 1) and find these steady states and their stability. In this context, we note that the tumour-present macrophage-present state is stable for the baseline parameter values in Table 1. Hence, it expected that the baseline numerical simulations will approach this state; see also Fig. 6(a)(i).*

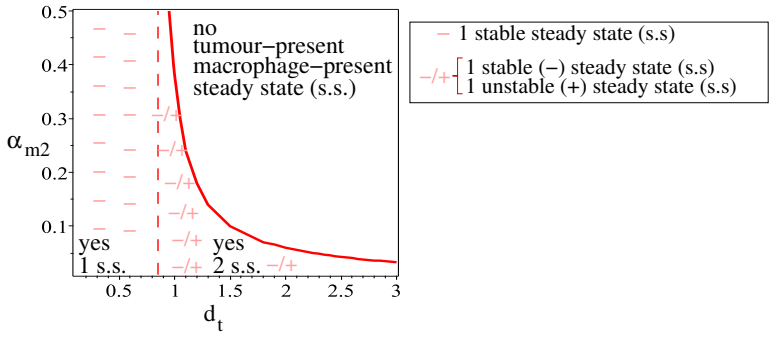

Fig. 9 Stability of the tumour-present/macrophage-present steady states (7) – when they exists – in the parameter space (d_t, α_{m2}). Here $\alpha_{m1} = 0.1$ and all other parameter values are as is Table 1. When only 1 steady state (s.s.) exists, it is always stable $(-)$; when 2 steady states co-exists, one is stable $(-)$ and the other one is unstable $(+)$.

Remark 3 *As mentioned in the main text, the steady state* $(0, M_1^* > 0, M_2^* > 0)$ *exists only when* $p_{m1} \neq p_{m2}$*. This can be easily seen if we solve (1b)-(1c) for* u_{M1}^* *and* u_{M2}^**:*

$$u_{M1}^* = \frac{\alpha_{m2} K_M \left[p_{m2} - (d_m + \alpha_{m2})\right]}{(\alpha_{m2} + d_m)(p_{m2} - p_{m1})},$$
$$u_{M2}^* = \frac{K_M \left[(\alpha_{m2} + d_m)(p_{m2} - p_{m1}) - \alpha_{m2} p_{m2}\right] \left[p_{m2} - (d_m + \alpha_{m2})\right]}{p_{m2}(\alpha_{m2} + d_m)(p_{m2} - p_{m1})}.$$

Note that both $u_{M1}^* > 0$ *and* $u_{M2}^* > 0$ *exist only if* $p_{m2} > \max\{p_{m1}, d_m + \alpha_{m2}\}$.
The case $p_{m1} = p_{m2} = p_m$ *reduces the steady-state equations (1b)-(1c) to the following expression (since* $1 - (u_{M1}^* + u_{M2}^*)/K_M = (\alpha_{m2} + d_m)/p_{m2}$*, and thus* u_{M1}^* *will disappear from the steady-state equation (1b)):*

$$0 = \alpha_{m2} K_M \left[p_{m2} - (d_m + \alpha_{m2})\right] \quad \Leftrightarrow \quad p_{m2} = d_m + \alpha_{m2}.$$

However, substituting the above right-hand-side expression into

$$u_{M2}^* = \frac{\left[p_{m2} - (d_m + \alpha_{m2})\right] K_M}{p_{m2}} - u_{M1}^*,$$

leads to $u_{M2}^* = -u_{M1}^*$*, which is not biologically realistic. Hence the steady state* $(0, u_{M1}^*, u_{M2}^*)$ *cannot exist when* $p_{m1} = p_{m2} = p_m$.
Since in this study we considered only the case $p_{m1} = p_{m2} =: p_m$ *(for simplicity, and to connect the results of the discrete-phenotype model (1) and the continuous-phenotype model (2); see Figs. 4(a) vs. 4(b)), here we chose to not discuss the stability of the tumour-free macrophages-present steady state.*

C Stability of steady states for model (2)

We now consider small perturbations of the phenotypically-homogeneous steady states u_T^* and u_M^* (i.e., $u_T(t) = u_T^* + a_1 e^{\sigma t}$, $\quad u_M(t, m) = u_M^* + a_2 e^{\sigma t + ikm}$). Substituting these perturbations into the linearised system (2) leads to

$$\begin{pmatrix} \sigma + B_{11} & B_{12} \\ 0 & \sigma + B_{22} \end{pmatrix} \begin{pmatrix} a_1 \\ a_2 \end{pmatrix} = 0, \quad \text{where}$$

$$B_{11} = d_t u_M^* - \big(1 + r_m u_M^*\big) p_t \Big(1 - \frac{2u_T^*}{K_T}\Big), \tag{11a}$$

$$B_{12} = d_t u_T^* \hat{H}_1(k) - p_t u_T^* \Big(1 - \frac{u_T^*}{K_T}\Big) r_m \hat{H}_2(k), \text{ with } \hat{H}_{1,2}(k) = \int_0^{L_m} H_{1,2}(m) e^{ikm} dm, \tag{11b}$$

$$B_{22} = ike^{-g_0 u_M^*} \Big(\alpha_{m1} \frac{u_T^*}{u_T^* + K_T^*} - \alpha_{m2} u_M^*\Big) + \frac{p_m}{K_M} u_M^* - p_m \Big(1 - \frac{u_M^*}{K_M}\Big) + d_m. \tag{11c}$$

This leads to the following characteristic equation:

$$\sigma^2 + \sigma\big(B_2 + B_1\big) + B_1 B_2 = 0,$$

with roots

$$\sigma_1 = -B_{11}, \quad \sigma_2 = -B_{22}.$$

First note that the kernels $H_1(m)$ and $H_2(m)$ (which appear only in B_{12}) do not influence these roots, and so the shape of the kernels (see Fig. 3) does not have any impact on the stability of the phenotype-homogeneous steady states. Second, note that the wavenumber k appears only in $\sigma_2 = -B_{22}$, and it does so in the complex part of this root. Hence, the steady states will be stable/unstable to an infinite range of wavenumbers.

Proposition 2 *Consider model (2) with the continuous macrophage phenotype, which can exhibit four phenotype-heterogeneous steady states.*

1. *The tumour-free macrophage-free steady state* $(u_T^*, u_M^*) = (0, 0)$ *is always unstable.*
2. *The tumour-free macrophage-present steady state* $(u_T^*, u_M^*) = (0, \frac{(p_m - d_m)K_M}{p_m})$ *is asymptotically stable if and only if* $p_m p_t < d_t K_M (p_m - d_m) - p_t r_m K_M (p_m - d_m)$.
3. *The tumour-present macrophage-free steady state* $(u_T^*, u_M^*) = (K_T, 0)$ *is unstable if* $p_m > d_m$.
4. *The tumour-present macrophage-present steady state* $(u_T^* > 0, u_M^* > 0)$ *is always asymptotically stable.*

Before discussing briefly how these stability results were obtained, note that the inequality for the stability of the tumour-free macrophage-present state is more restrictive than the inequality for the stability of the discrete-phenotype steady state $(0, (p_m - d_m)K_M/pm, 0)$. This is explained by the difference in the steady states: the phenotypically-discrete states have $u_{M2}^* = 0$, while the phenotypically-continuous states incorporate both u_{M1}^* and u_{M2}^* and thus they can be de-stabilised by increasing the M2 sub-population.

Proof:

1. At the trivial state $(0, 0)$, the roots of the characteristic equation are $\sigma_1 = p_t > 0$ and $\sigma_2 = (p_m - d_m)$, and therefore this state is always unstable .
2. At the state $(0, \frac{(p_m - d_m)K_M}{p_m})$, which exists only if $p_m > d_m$, the roots of the characteristic equation are

$$\sigma_1 = p_t + (p_t r_m - d_t) \frac{(p_m - d_m)K_M}{p_m}, \tag{12}$$

$$\sigma_2 = -(p_m - d_m) + ike^{-g_0 K_M (p_m - d_m)/p_m} \alpha_{m2} \frac{(p_m - d_m)K_M}{p_m}, \tag{13}$$

   and therefore the steady state is asymptotically stable when $\sigma_1 < 0$, which leads to the required inequality.
3. At the state $(K_T, 0)$, the roots of the characteristic equation are $\sigma_1 = -p_t < 0$ and $Re(\sigma_2(k)) = p_m - d_m > 0$, and thus this state is always unstable.

4. At the steady state ($u_T^* > 0, u_M^* > 0$), which exists only for $(p_m - d_m) > 0$ and $d_t - p_t r_m < \frac{p_m p_t}{(p_m - d_m)K_M}$, we have $Re(\sigma_2(k)) = -(p_m - d_m) < 0$. Thus the stability is controlled by σ_1:

$$\sigma_1 = \frac{(-p_t r_m + d_t)(p_m - d_m)K_M - p_m p_t}{p_m} < 0 \quad \Leftrightarrow \quad d_t - p_t r_m < \frac{p_m p_t}{(p_m - d_m)K_M}.$$

This last inequality coincides with the inequality for the existence of this state (see equation (8b)), and thus the state is asymptotically stable whenever it exists.

Fig. 10 shows the real and imaginary parts of σ_1 and σ_2 for wavenumber $k < 100$ and $d_t = 0.5$ (continuous lines) and $d_t = 1.0$ (dash-dot lines). As discussed above, increasing d_t can lead to unstable states; however this instability is characterised by an infinite number of wavenumbers k becoming unstable at the same time (and the corresponding positive eigenvalues $\sigma(k)$).

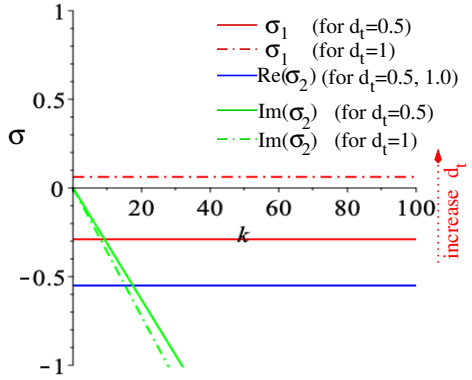

Fig. 10 Dispersion relation $\sigma_{1,2}(k)$, corresponding to the phenotypically-homogeneous steady state ($u_T^* > 0, u_M^* > 0$) given by equations (8), as we vary the rate d_t at which M1-like macrophages eliminate the tumour cells.

D The impact of different shapes of phenotype kernels

We have seen in Fig. 8 that an overlap in the macrophages phenotype leads to a delay in the killing and relapse of tumour cells. There, we considered phenotype kernels that put similar emphasis on cells with M1 and M2 phenotypes. Here we investigate what happens if we change the shape of the phenotype kernel, and put more emphasis on the cells with more extreme phenotypes (e.g., on the M1 macrophages with a phenotype $m < 3$, and on the M2 macrophages with a phenotype $m > 7$). In Fig. 11(i) we depict two such types of kernels:

$$\text{(i) } H_1(m) = me^{-m}, \quad H_2(m) = (L_m - m)e^{-(L_m - m)}, \text{ and} \tag{14a}$$

$$\text{(ii) } H_1(m) = \frac{m}{1+\epsilon}e^{-\frac{m}{1+\epsilon}}, \quad H_2(m) = \frac{(L_m - m)}{1+\epsilon}e^{-\frac{(L_m - m)}{1+\epsilon}}, \text{ with } \epsilon = 0.3. \tag{14b}$$

Comparing Fig 11(ii) with Fig. 7(b)(i), we see that the shape of the kernels does have an impact on the level of tumour reduction by the M1 cells (when we keep all other model parameters and initial conditions fixed). In particular, kernels (14) lead to a much smaller reduction in tumour population compared to kernels (5)-(6).

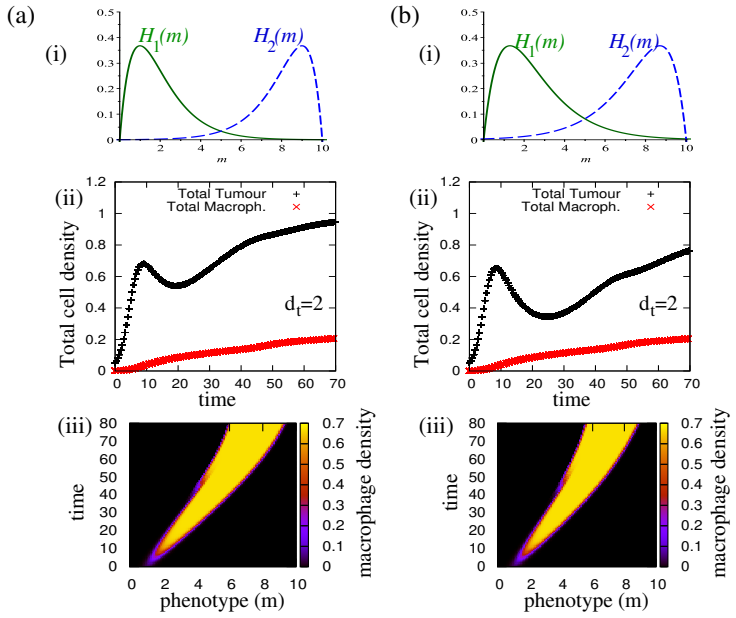

Fig. 11 Dynamics of system (2) with: (a) kernels (14a), and (b) kernels (14b), as we vary the degree of overlap between H_1 and H_2. Here, $p_m = 0.7$, $p_t = 0.6$, $\alpha_{m1} = 0.1$, $\alpha_{m2} = 0.01$, $d_t = 2.0$, and the rest of the parameters are as in Table 1.

Various other types of kernels, with or without overlap, could be used to model macrophages phenotype. An extreme type of such kernel without overlap can be described by a delta function, which would allow us to reduce the non-local terms for continuous phenotype to local terms describing the interactions between the discrete M1 and M2 phenotypes, and thus compare models (1) and (2). However, since the goal of this study is not to focus on more models with discrete phenotype, but rather to investigate the impact of M1/M2 mixed phenotype on tumour outcomes, we leave such a comparison for a future study.

References

1. Allavena, P., Mantovani, A.: Immunology in the clinic review series; focus on cancer: tumour-associated macrophages: undisputed stars of the inflammatory tumour microenvironment. Clinical and Experimental Immunology **167**, 195–205 (2012)
2. Aras, S., Zaidi, M.R.: TAMeless traitors: macrophages in cancer progression and metastasis. British Journal of Cancer **117**, 1583–1591 (2017)
3. Bardi, G., Smith, M., Hood, J.: Melanoma exosomes promote mixed M1 and M2 macrophage polarisation. Cytokine **105**, 63–72 (2018)
4. den Breems, N., Eftimie, R.: The re-polarisation of M2 and M1 macrophages and its role on cancer outcomes. J. Theor. Biol. **390**, 23–39 (2016)
5. Bridle, B., Stephenson, K., Boudreau, J., Koshy, S., Kazdhan, N., Pullenayegum, E., Brunellière, J., Bramson, J., Lichty, B., Wan, Y.: Potentiating cancer immunotherapy using an oncolytic virus. Mol. Ther. **18**(8), 1430–1439 (2010)
6. Burkholder, B., Huang, R.Y., Burgess, R., Luo, S., Jones, V., Zhang, W., Lv, Z.Q., Gao, C.Y., Wang, B.L., Zhang, Y.M., Huang, R.P.: Tumor-induced perturbations of

cytokines and immune cell networks. Biochimica et Biophysica Acta **1845**(2), 182–201 (2014)
7. Cai, X., Yin, Y., Li, N., Zhu, D., Zhang, J., Zhang, C.Y., Zen, K.: Re-polarisation of tumour-associated macrophages to pro-inflammatory M1 macrophages by microRNA-155. J. Molecular Cell Biology **4**(5), 341–343 (2012)
8. Celada, A.: Inflammation and macrophages. In: IRB Barcelona. 2008 Scientific Report, pp. 78–82. IRB Barcelona (2008)
9. Chen, P., Huang, Y., Bong, R., Ding, Y., Song, N., Wang, X., Song, X., Luo, Y.: Tumour-associated macrophages promote angiogenesis and melanoma growth via adrenomedullin in a paracrine and autocrine manner. Clin. Cancer Res. **17**(23), 7230–7239 (2011)
10. Chitu, V., Yeung, Y.G., Yu, W., Nandl, S., Stanley, E.: Measurement of macrophage growth and differentiation. Curr. Protoc. Immunol. pp. 1–26 (2011)
11. Condeelis, J., Pollard, J.: Macrophages: obligate partners for tumour cell migration, invasion, and metastasis. Cell **124**, 263–266 (2006)
12. van Dalen, F., van Stevendaal, M., Fennemann, F., Verdoes, M., Ilina, O.: Molecular repolarisation of tumour-associated macrophages. Molecules **24**, 9 (2019)
13. DeVita, V., Young, R., Canellos, G.: Combination versus single agent chemotherapy: a review of the basis for selection of drug treatment for cancer. Cancer **35**, 98–110 (1975)
14. DuPré, S., Redelman, D., Jr., K.H.: The mouse mammary carcinoma 4T1: characterisation of the cellular landscape of primary tumours and metastatic tumour foci. Int. J. Exp. Path. **88**, 351–360 (2007)
15. Eftimie, R., Eftimie, G.: Tumour-associated macrophages and oncolytic virotherapies: a mathematical investigation into a complex dynamics. Letters in Biomathematics **5**(1), S6–S35 (2018)
16. Eftimie, R., Hamam, H.: Modelling and investigation of the $CD4^+$ T cells - Macrophages paradox in melanoma immunotherapies. J. Theor. Biol. **420**, 82–104 (2017)
17. Endo, H., Inoue, M.: Dormancy in cancer. Cancer Sci. **110**(2), 474–480 (2019)
18. Eubank, T., Roberts, R., Khan, M., Curry, J., Nuovo, G., Kuppusamy, P., Marsh, C.: Granulocyte macrophage colony-stimulating factor inhibits breast cancer growth and metastasis by invoking an anti-angiogenic program in tumour-educated macrophages. Cancer Res. **69**(5), 2133–2140 (2009)
19. Fidler, I.: Macrophages and metastasis: a biological approach to cancer therapy: presidential address. Cancer Research **45**, 4714–4726 (1985)
20. Fidler, I., Barnes, Z., Fogler, W., Kirsh, R., Bugelski, P., Poste, G.: Involvement of macrophages in the eradication of established metastases following intravenous injection of liposomes containing macrophage activators. Cancer Res. **42**, 496–501 (1982)
21. Fraternale, A., Brundu, S., Magnani, M.: Polarisation and repolarisation of macrophages. J. Clin. Cell Immunol. **6**(2), 319 (2015)
22. Friberg, S., Mattson, S.: On the growth rates of human malignant tumoursl implications for medical decision making. J. Surgical Oncology **65**, 284–297 (1997)
23. Gao, X., Wang, X., Yang, Q., Zhao, X., Wen, W., Li, G., Lu, J., Qin, W., Qi, Y., Xie, F., Jiang, J., Wu, C., Zhang, X., Chen, X., Turnquist, H., Zhu, Y., Lu, B.: Tumoural expression of IL-33 inhibits tumour growth and modifies the tumour microenvironment through $CD8^+$T and NK Cells. J. Immunol. **194**, 438–445 (2015)
24. Genard, G., Lucas, S., Michiels, C.: Reprogramming of tumour-associated macrophages with anticancer therapies: radiotherapy versus chemo- and immunotherapies. Front. Immunol. **8**, 828 (2017)
25. Georgoudaki, A.M., Prokopec, K., Boura, V., Hellqvist, E., Sohn, S., J.Östling, Dahan, R., Harris, R., Rantalainen, M., Klevebring, D., Sund, M., Brage, S.E., Fuxe, J., Rolny, C., Li, F., Ravetch, J., Karlsson, M.: Reprogramming tumour-associated macrophages by antibody targeting inhibits cancer progression and metastasis. Cell Reports **15**, 2000–2011 (2016)
26. Ginhoux, F., Jung, S.: Monocytes and macrophages: developmental pathways and tissue homeostasis. Nat. Rev. Immunol. **14**, 392–404 (2014)
27. Gordon, S., Maute, R., Dulken, B., Hutter, G., George, B., McCracken, M., Gupta, R., Tsai, J., Sinha, R., Corey, D., A.M.Ring, Connolly, A., Weissman, I.: PD-1 expression by tumour-associated macrophages inhibits phagocytosis and tumour immunity. Nature **545**(7655), 495–499 (2017)

28. Gregório, A., Fonseca, N., Moura, V., Lacerda, M., Figueiredo, P., SimÖes, S., Moreira, J.: Inoculated cell density as a determinant factor of the growth dynamics and metastatic efficiency of a breast cancer murine model. PLoS One **11**(11), e0165817 (2016)
29. Gül, N., van Egmond, M.: Antibody-dependent phagocytosis of tumour cells by macrophages: a potent effector mechanism of monoclonal antibody therapy of cancer. Cancer Res. **75**(23), 5008 –5013 (2015)
30. Hanahan, D., Weinberg, R.: Hallmarks of cancer: the next generation. Cell **144**(5), 646–674 (2011)
31. He, Y.F., Zhang, M.Y., Wu, X., Sun, X.J., Xu, T., He, Q.Z., Di, W.: High MUC2 expression in ovarian cancer is inversely associated with the M1/M2 ratio of tumour-associated macrophages and patient survival time. PLoS ONE **8**(12), e79769 (2013)
32. Heusinkveld, M., van der Burg, S.: Identification and manipulation of tumour associated macrophages in human cancers. J. Translational Medicine **9**, 216 (2011)
33. Jadus, M., Irwin, M., Irwin, M., Horansky, R., Sekhon, S., Pepper, K., Kohn, D., Wepsic, H.: Macrophages can recognise and kill tumour cells bearing the membrane isoform of macrophage colony-stimulating factor. Blood **87**(12), 5232–5241 (1996)
34. Josephs, D., Bax, H., Karagiannis, S.: Tumour-associated macrophage polarisation and re-education with immunotherapy. Front. Biosci. (Elite Ed.) **7**, 293–308 (2015)
35. Karnevi, E., Anderson, R., Rosendahl, A.: Tumour-educated macrophages display a mixed polarisation and enhance pancreatic cancer cell invasion. Immunology and Cell Biology **92**(6), 543–552 (2014)
36. Laird, A.: Dynamics of tumor growth. Br. J. Cancer **18**, 490–502 (1964)
37. Laird, A.: Dynamics of relative growth. Growth **29**, 249–263 (1965)
38. Li, Q., Hao, Z., He, W., Zhao, W.: Reprogramming tumour associated macrophage phenotype by a polysaccharide from *Ilex asprella* for sarcoma immunotherapy. Int. J. Mol. Sci. **19**(12), E3816 (2018)
39. Li, X., Jolly, M., George, J., Pienta, K., Levine, H.: Computational modelling of the crosstalk between macrophage polarisation and tumour cell plasticity in the tumour microenvironment. Frontiers in Oncology **9**, 10 (2019)
40. Louzoun, Y., Xue, C., Lesinski, G., Friedman, A.: A mathematical model for pancreatic cancer growth and treatments. J. Theor. Biol. **351**, 74–82 (2014)
41. Luo, Y., Zhou, H., Krueger, J., Kaplan, C., Liao, D., Markowitz, D., Liu, C., Chen, T., Chuang, T.H., Xiang, R., Reisfeld, R.: The role of proto-oncogene Fra-1 in remodelling of the tumour microenvironment in support of breast tumour cell invasion and progression. Oncogene **29**(5), 662–673 (2010)
42. Ma, J., Liu, L., Che, G., Yu, N., Dai, F., You, Z.: The M1 form of tumour-associated macrophages in non-small cell lung cancer is positively associated with survival time. BMC Cancer **10**, 112–120 (2010)
43. Madera, L., Greenshields, A., Coombs, M.P., Hoskin, D.: 4T1 murine mammary carcinoma cells enhance macrophage-mediated innate inflammatory responses. PLoS One **10**(7), e0133385 (2015)
44. Mahlbacher, G., Curtis, L., Lowengrub, J., Frieboes, H.: Mathematical modelling of tumour-associated macrophage interactions with the cancer microenvironment. J. Immunother. Cancer **6**, 10 (2018)
45. Makela, A., Gaudet, J., Foster, P.: Quantifying tumour associated macrophages in breast cancer: a comparison of iron and fluorine-based MRI cell tracking. Sci. Rep. **7**, 42109 (2017)
46. Mantovani, A., Biswas, S., Galdiero, M., Sica, A., Locati, M.: Macrophage plasticity and polarisation in tissue repair and remodelling. J. Pathol. **229**, 176–185 (2013)
47. Mantovani, A., Sozzani, S., Locati, M., Allavena, P., Sica, A.: Macrophage polarisation: tumour-associated macrophages as a paradigm for polarised M2 mononuclear phagocytes. TRENDS in Immunology **23**(11), 549–555 (2002)
48. Martinez-Marin, D., Jarvis, C., Nelius, T., Filleur, S.: Assessment of phagocytic activity in live macrophages-tumour cells co-cultures by confocal and Nomarski microscopy. Biology Methods and Protocols **2**(1), 1–7 (2017)
49. Matovani, A., Marchesi, F., Malesci, A., Laghi, L., Allavena, P.: Tumour-associated macrophages as treatment targets in oncology. Nat. Rev. Clin. Oncol. **14**, 399–416 (2017)

50. McCabe, A., MacNamara, K.: Macrophages: key regulators of steady state and demand-adapted hematopoiesis. Exp. Hematol. **44**(4), 213–222 (2016)
51. Monte, U.D.: Does the cell number 10^9 still really fit one gram of tumour tissue? Cell Cycle **8**(3), 505–506 (2009)
52. Morales, V., Soto-Ortiz, L.: Modelling macrophage polarisation and its effect on cancer treatment success. Open Journal of Immunology **8**(2), 36–80 (2018)
53. Mosoyan, G., Nagi, C., Marukian, S., Teixeira, A., Simonian, A., Resnick-Silverman, L., DiFeo, A., Johnston, D., Reynolds, S., Roses, D., Mosoian, A.: Multiple breast cancer cell-lines derived from a single tumour differ in their molecular characteristics and tumorigenic potential. PLoS ONE **8**(1), e55145 (2013)
54. Movahedi, K., Laoui, D., Gysemans, C., Baeten, M., Stangé, G., den Bossche, J.V., Mack, M., Pipeleers, D., Veld, P.I., Baetselier, P.D., Ginderachter, J.V.: Different tumour microenvironments contain functionally distinct subsets of macrophages derived from Ly6C(high) monocytes. Cancer Res. **70**(14), 5728–5739 (2010)
55. Nakamura, T., Kamogawa, Y., Bottomly, K., Flavell, R.: Polarisation of IL-4 and IFN-gamma-producing $CD4^+$ T cells following activation of naive $CD4^+$ T cells. J. Immunol. **158**(3), 1085–1094 (1997)
56. Ohri, C., Shikotra, A., Green, R., Waller, D., Bradding, P.: Macrophages within NSCLC tumour islets are predominantly of a cytotoxic M1 phenotype associated with extended survival. Eur. Respir. J. **33**, 118–126 (2009)
57. Phan, T., Tian, J.: The role of the innate immune system in oncolytic virotherapy. Computational and Mathematical Methods in Medicine **2017**, 6587258 (2017)
58. Pulaski, B., Ostrand-Rosenberg, S.: Mouse 4T1 breast tumour model. Current Protocols in Immunology **39**(1), 21.2.1–20.2.16 (2000)
59. Reinartz, S., Schumann, T., Finkernagel, F., Wortmann, A., Jansen, J., Meissner, W., Krause, M., Schwörer, A., Wagner, U., Müller-Brüsselbach, S., Müller, R.: Mixed-polarisation phenotype of ascites-associated macrophages in human ovarian carcinoma: correlation of CD163 expression, cytokine levels and early relapse. Int. J. Cancer. **134**(1), 32–42 (2014)
60. Riabov, V., Kim, D., Chhina, S., Alexander, R., Klyushnenkova, E.: Immunostimulatory early phenotype of tumour-associated macrophages does not predict tumour growth outcome in an HLA-DR mouse model of prostate cancer. Cancer Immunol. Immunother. **64**(7), 873–883 (2015)
61. Shaw, T., Houston, S., Wemyss, K., Bridgeman, H., Barbera, T., Zangerle-Murray, T., Strangward, P., Ridley, A., Wang, P., Tamoutounour, S., Allen, J., Konkel, J., Grainger, J.: Tissue-resident macrophages in the intestine are long lived and defined by Tim-4 and CD4 expression. Journal Experimental Medicine **215**(6), 1507 (2018)
62. Sica, A., Larghia, P., Mancino, A., Rubino, L., Porta, C., Totaro, M., Rimoldi, M., Biswas, S., Allavena, P., Mantovani, A.: Macrophage polarisation in tumour progression. Seminars in Cancer Biology **18**, 349–355 (2008)
63. Singhal, S., Stadanlick, J., Annunziata, M., Rao, A., Bhojnagarwala, P., O'Brien, S., Moon, E., Cantu, E., Danet-Desnoyers, G., Ra, H.J., Litzky, L., Akimova, T., Beier, U., Hancock, W., Albelda, S., Eruslanov, E.: Human tumor-associated monocytes/macrophages and their regulation of T cell responses in early-stage lung cancer. Scie. Transl. Med **11**(479), eaat1500 (2019)
64. Sousa, S., Brion, R., Lintunen, M., Kronqvist, P., Sandholm, J., Mönkkönen, J., Kellokumpu-Lehtinen, P.L., Lauttia, S., Tynnien, O., Joensuu, H., Heymann, D., Määttä, J.: Human breast cancer cells educate macrophages toward the M2 activation status. Breast Cancer Research **17**, 101 (2015)
65. Strachan, D., Ruffell, B., Oei, Y., Bissell, M., Coussens, L., N.Pryer, Daniel, D.: CSF1R inhibition delays cervical and mammary tumour growth in murine models by attenuating the turnover of tumour-associated macrophages and enhancing infiltration by $CD8^+$ T cells. OncoImmunology **2**(12), e26968–1 – e26968–12 (2013)
66. Vallerand, D., Massonnet, G., Kébir, F., Gentien, D., Maciorowski, Z., la Grange, P.D., Sigal-Zafrani, B., Richardson, M., Humbert, S., Thuleau, A., Assayag, F., de Plater, L., Nicolas, A., Scholl, S., Marangoni, E., Weigand, S., Roman-Roman, S., Savina, A., Decaudin, D.: Characterisation of breast cancer preclinical models reveals a specific pattern of macrophage polarisation. PLoS One **11**(7), e0157670 (2016)

67. Wang, H.F., Wang, S.S., Huang, M.C., Liang, X.H., Tang, Y., Tang, Y.: Targeting immune-mediated dormancy: a promising treatment for cancer. Front. Oncol. **9**, 498 (2019)
68. Yan, H., Jiang, J., Pang, Y., Achyut, B., Lizardo, M., Liang, X., Hunter, K., Khanna, C., Hollander, C., Yang, L.: CCL9 induced by TGFβ signalling in myeloid cells enhances tumour cell survival in the premetastatic organ. Cancer Research **75**(24), 5283–5298 (2015)
69. Yang, M., Ma, B., Shao, H., Clark, A., Wells, A.: Macrophage phenotypic subtypes diametrically regulate epithelial-mesenchymal plasticity in breast cancer cell. BMC Cancer **16**, 419 (2016)
70. Yang, M., McKay, D., Pollard, J., Lewis, C.: Diverse functions of macrophages in different tumour microenvironments. Cancer Research **78**(19), 5492–5503 (2018)
71. Zhang, X., Tian, W., Cai, X., Wang, X., Dang, W., Tang, H., Cao, H., Wang, L., Chen, T.: Hydrazinocurcumin encapsulated nanoparticles "re-educate" tumour-associated macrophages and exhibit anti-tumour effects on breast cancer following STAT3 suppression. PLoS One **8**(6), e65896 (2013)
72. Zheng, H., Zou, W., Shen, J., Xu, L., Wang, S., Fu, Y.X., Fan, W.: Opposite effects of coinjection and distant injection of mesenchymal stem cells on breast tumour cell growth. Stem Cells Translational Medicine **5**, 1216–1228 (2016)